ELSEVIER

Int. J. Therm. Sci. 41 (2002) 609–618

International Journal of Thermal Sciences

www.elsevier.com/locate/ijts

A photographic study on the near-wall bubble behavior in subcooled flow boiling ☆

Soon Heung Chang [a,*], In Cheol Bang [a], Won-Pil Baek [b]

[a] *Korea Advanced Institute of Science and Technology, 373-1, Guseong-dong , Yuseong-gu, Daejeon, 305-701, Republic of Korea*
[b] *Korea Atomic Energy Research Institute, 150, Dukjin-dong, Yuseong-gu, Daejeon, 305-353, Republic of Korea*

Received 26 October 2001; received in revised form 8 February 2002

Abstract

The behavior of near-wall bubbles in subcooled flow boiling has been investigated photographically for water flow in vertical, one-side heated, rectangular channels at mass fluxes of 500, 1500, 2000 $kg \cdot m^{-2} \cdot s^{-1}$ under atmospheric pressure. Primary attention was given to the bubble coalescence phenomenon and the structure of the near-wall bubble layer. The number of near-wall bubbles increased with the increase in the heat flux. At sufficiently high heat fluxes (>60–70% CHF), three characteristic layers were observed in the heated channel:

(a) a superheated liquid layer with small bubbles attached on the heated wall,
(b) a flowing bubble layer consisting of large coalesced bubbles over the superheated liquid layer, and
(c) the liquid core over the flowing bubble layer. In addition, the existence of a liquid sublayer under coalesced bubbles was identified photographically.

According to visualization, the CHF mechanism for the present experimental condition could be related to the formation of large vapor clots resulting from coalescences of bubbles and the evaporation of the superheated liquid layer beneath those clots.

Keywords: CHF; Liquid sublayer; Bubble; Flow structure; Visualization

1. Introduction

Forced convective nucleate boiling is very effective in achieving a high heat flux with a small temperature difference between the heated surface and the cooling fluid; however, there is a boundary of this effective heat transfer regime, called the departure from nucleate boiling (DNB). Reliable understanding of this DNB phenomenon is important for effective and safe operation of nuclear systems and other thermal-hydraulic equipment [1,2].

DNB is a transition of the heat transfer regime from nucleate boiling to film boiling or partial film boiling. This usually involves the transition of the flow regime from bubbly flow to inverted annular flow. Detailed physical mechanisms leading to DNB, however, have not been clearly understood in spite of extensive research, mainly due to the difficulty in observing the near-wall region. Several investigators have tried to get rid of this difficulty by means of various flow visualization tests. Their works have focused mainly on bubble parameters within the bubble boundary layer and bubble behavior related to DNB occurrence. Gunther [3] investigated bubble growth-collapse process and measured maximum bubble size, population and growth rate, etc. It was also reported that when the local vapor film due to bubbles coalescence was formed, the CHF would occur. Jiji and Clark [4] investigated the bubble boundary layer and correlated its thickness. Tong et al. [5] identified the effect of mass flow rate on bubble size and correlated the bubble size for freon-113. In particular, they suggested the existence of a superheated liquid layer on the heated wall. Galloway and Mudawwar [7] suggested that one of the

☆ This article is a follow-up a communication presented by the authors at the ExHFT-5 (5th World Conference on Experimental Heat Transfer, Fluid Mechanics and Thermodynamics), held in Thessaloniki in September 24–28, 2001.

* Correspondence and reprints.
E-mail addresses: shchang@mail.kaist.ac.kr (S.H. Chang), wpbaek@kaeri.re.kr (W.-P. Baek).

1290-0729/02/$ – see front matter
PII: S1290-0729(02)01354-6

Nomenclature

C_p	specific heat	$J \cdot kg^{-1} \cdot K^{-1}$
D	thermocouple outer diameter	mm
G	mass flux	$kg \cdot m^{-2} \cdot s^{-1}$
h	heat transfer coefficient	$W \cdot m^{-2} \cdot K^{-1}$
k	thermal conductivity	$W \cdot m^{-1} \cdot K^{-1}$
t	heater thickness	m
T	temperature	°C
$T(x)$	temperature at distance x	°C
x	distance from inner surface	m
Xe	thermodynamic quality	
P	pressure	bar

Greek symbol

ΔT_{sat}	wall superheat ($T_w - T_{sat}$)	°C
ΔT_{sub}	subcooling ($T_{sat} - T_f$)	°C
ϕ	heat flux	$MW \cdot m^{-2}$

Subscripts

e	exit
w	wall
f	fluid
i	inlet
l	liquid
s	heater surface
sub	subcooling
sat	saturation

wetting fronts was dried out due to the radial inertia of vapor related to wavelike succession of vapor clots at CHF.

Various mechanisms have been reported as the primary causes of DNB but any theoretical models with good prediction performance are not tightly linked to such reported experimental results [8]. Weisman and Pei [9] postulated that CHF occurred when the volume fraction of steam in the bubbly layer just exceeded a critical void fraction. However, Lee and Mudawwar [6] postulated that CHF occurs as a result of the Helmholtz instability if the heat flux is sufficient for microlayer dryout below vapor blanket.

Digital photographic techniques have significantly advanced for recent decades. This would enable researchers to overcome some difficulties of visualization study in relation to complex boiling phenomena.

In this study, by using digital photographic techniques, boiling characteristics and flow structure have been examined for the subcooled flow boiling of water in a vertical rectangular channel with one-side heating.

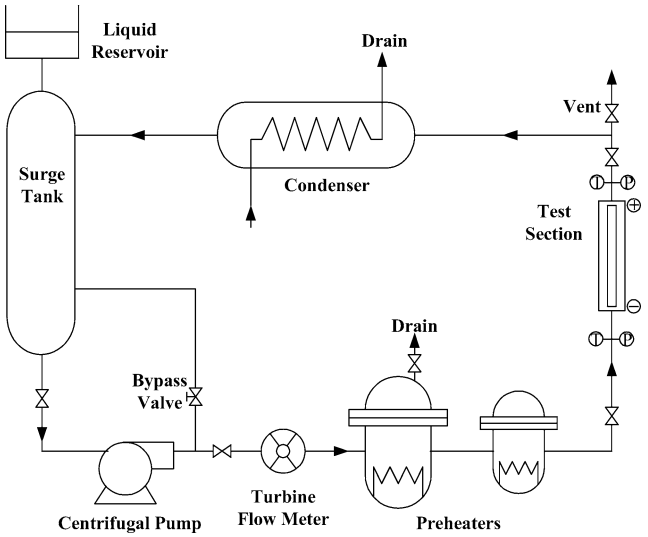

Fig. 1. Schematics of the experimental loop.

2. Experimental method

2.1. Experimental loop and test section

Subcooled flow boiling tests have been performed with water at a pressure of 1.13 bar ($T_{sat} = 103\,°C$), for mass fluxes of 500, 1500, 2000 $kg \cdot m^{-2} \cdot s^{-1}$ and inlet subcooling of 50 °C. Fig. 1 shows the schematic of the experimental loop that consists of the following components: a centrifugal pump, a turbine flow-meter, two pre-heaters, a test section, a condenser, a surge tank and a liquid reservoir. Electrical power is provided to the test section by a DC power supplier with the maximum capacity of 64 kW (32 V and 2000 A).

A vertical, one-side heated rectangular channel has been used as the test section, as shown in Fig. 2. It consists of two components: a channel body and an inserter containing a heating plate. The body is made of aluminum alloy and provides a flow channel of 8 mm (width including the heated surface) × 5 mm (height with window), and Lexan windows for visualization from front and side parts. The inserter is made of Bakelite as an insulator and a stainless steel heating plate with the size of 4 mm (width) × 100 mm (length) × 1.9 mm (thickness). The plate is heated by the DC power that is supplied through copper electrodes connected at both ends. The Bakelite insulator assures sufficient insulation allowing only a negligible heat loss (below a few $kW \cdot m^{-2}$) to the surrounding air.

To measure the heater surface temperature, two type K thermocouples are embedded in the heating plate of SS304 at the positions of 1 mm and 9 mm from the leading edge (i.e., the top of the heated section), and 0.4 mm in depth from the heated surface. The measurement of temperature

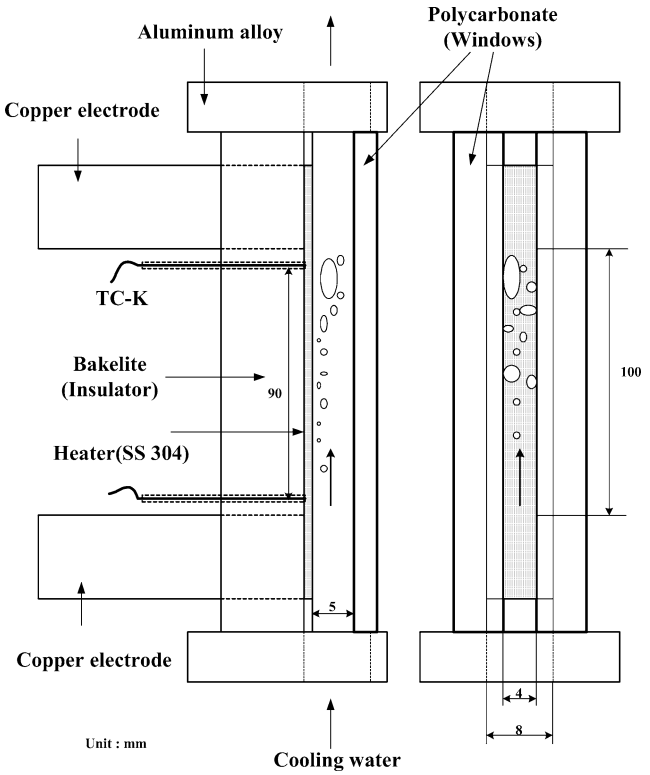

Fig. 2. Test section.

on the heated surface is corrected by using the heat diffusion equation:

$$T_s = T(x) - \frac{\phi t}{2k}\left(1 - \frac{x^2}{t^2}\right) \quad (1)$$

Its application method and embedding of a thermocouple are shown as Fig. 3.

Before performing tests, non-condensible gases dissolved in water are removed by circulating water for about an hour while maintaining water temperature above 95 °C by preheaters. After this operation, the water subcooling at the test section inlet is maintained at a fixed value (50 °C in the present experiment) automatically by controlling the power of preheaters and the cooling water flow into the condenser.

2.2. Visualization method

Visualization of the flow channel has been achieved by the aid of a still camera and a high-speed camera from the sides and the front. A Kodak Ektapro 1000 motion analyzer as a high-speed camera was used at speeds of 500 and 1000 frames per second but clear images could not be acquired due to poor resolution and low speed. Still photographs were taken originally with a Nikon FM2 camera. A Nikon D1 digital camera with total 2.74 million pixels (record pixels 2000 × 1312 which is used really) and flash-synchronized shutter speed of 1/500 second is finally used with considering the speed and advanced image resolution, which provide the spatial resolution of ∼10 μm per pixel to the images of this visual test.

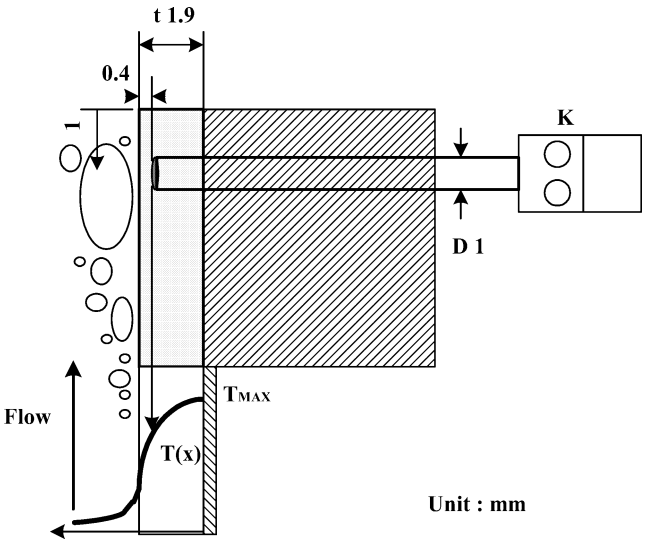

Fig. 3. Measurement of heater temperature.

Photographic technique that controls the exposure time by the flash speed is adopted for acquiring the clear still image of fast bubbles and disturbed boiling states. While the shutter is open, a high-speed flash of 1/8700 second is emitted to the flow channel. Additional backlighting is provided through a tracing paper in cases of lateral observation. The light source is a Nikon Speedlight SB-28 model. Fig. 4 illustrates the photographic system used in this work.

Nikon 105 mm micro lens and three extension tubes of 14 mm, 21 mm and 31 mm for close-up have been used to magnify the phenomena occurring in the flow channel. The focusing of the camera is fixed on the heating surface for front observation and the middle point of the flow width for side observation. Three Halogen lamps (2 × 300 W and 500 W) as the light source are also set near visual windows. After the capture of a bubble motion, image processing is performed mainly on the brightness and contrast of an image. In some cases, continuous photos are taken at the time interval of 0.22 second. In addition, photos are also taken with a relatively long exposure time in order to distinguish flowing bubbles and growing bubbles.

3. Results and discussion

Visualization of the near-wall region has enabled to identify the flow structure up to the range of several tens of microns. Simultaneous front and lateral observations were tried first, but it provided low-quality photographs due to the difficulty in providing proper lighting for both directions. Therefore, front observation was made first and lateral observation followed at similar conditions. Experimental conditions are summarized in Table 1.

The photographs obtained in this work have different characteristics according to the method of lighting even for the same conditions of mass flux, heat flux and subcooling.

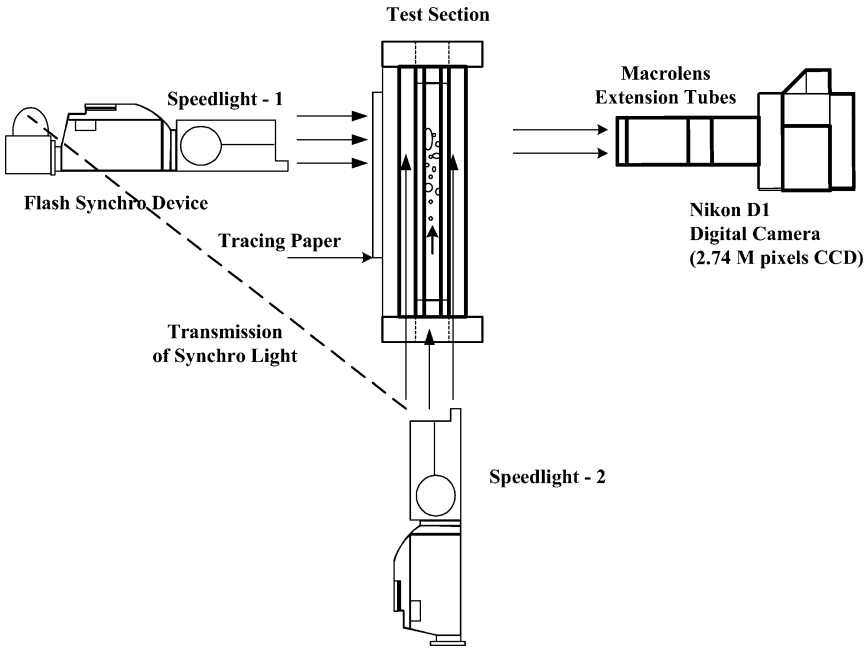

Fig. 4. Illustration of the photographic system.

Table 1
Experimental condition

	P	T_i	$\Delta T_{\text{sub,e}}$	G	ϕ
Front observation	1.13	53	36–50	500	0.334−3.3
	($T_{\text{sat}} = 103\,^{\circ}\text{C}$)			1500	1.45−6.4 (CHF)
				2000	2.3−8.4 (CHF)
Lateral observation	1.13	53	36–50	500	0.333−3.3
	($T_{\text{sat}} = 103\,^{\circ}\text{C}$)			1500	2.0−5.9
				2000	1.216−6.0

For example, back lighting and front lighting give clear images for near-wall (i.e., stationary) bubbles while lateral lighting for flowing bubbles. The overlapping of flowing bubbles and vapor clots over the heated surface gives the disorder to the spatial depth.

3.1. Boiling curves and experimental conditions

The boiling curves measured in experiment are shown in Fig. 5. The heat flux was estimated directly from the applied power. The inner surface temperature was calculated by applying Eq. (1) to the measured temperature at 0.4 mm distance from the surface ("corrected" in Fig. 5 mean these calculated values). The boiling curves are also compared with traditional heat transfer equations:

- McAdams et al. [10] equation for single-phase heat transfer

$$h_{\text{l}} = 0.023 \frac{k_{\text{f}}}{D_{\text{h}}} \left(\frac{G D_{\text{h}}}{\mu_{\text{f}}} \right)^{0.8} \left(\frac{C_{\text{p}} D_{\text{h}}}{k} \right)_{\text{f}}^{0.4} \tag{2}$$

– Thom et al. [11] correlation for fully-developed nucleate boiling

$$\Delta T_{\text{sat}} = 22.65 \phi^{0.5}\, \text{e}^{-p/87} \tag{3}$$

It is found that the heat flux versus surface temperature behavior measured in this work is consistent with the predictions by conventional correlations for circular tubes. Therefore, the measured boiling curve can be used in analyzing the observed phenomena though there might be some errors in the calculated surface temperature.

Fig. 6 indicates experimental conditions where visualization tests have been conducted. Visualization was conducted up to CHF condition for mass fluxes of 1500 $\text{kg}\cdot\text{m}^{-2}\cdot\text{s}^{-1}$ to investigate the overall behavior, then additional tests with other mass fluxes were conducted mainly to investigate the mass flux effect and to observe the superheated liquid layer under flowing bubbles.

3.2. Overall bubble behavior on the heated surface

Fig. 7 illustrates the development of the bubble layer along the heated length for varying heat fluxes. Fig. 8 shows the magnified photos for the exit (top) region. The quality shown in the figures is the thermodynamic equilibrium quality averaged for the cross section near the channel exit, which is calculated based on the inlet mass flux, inlet enthalpy and heat input.

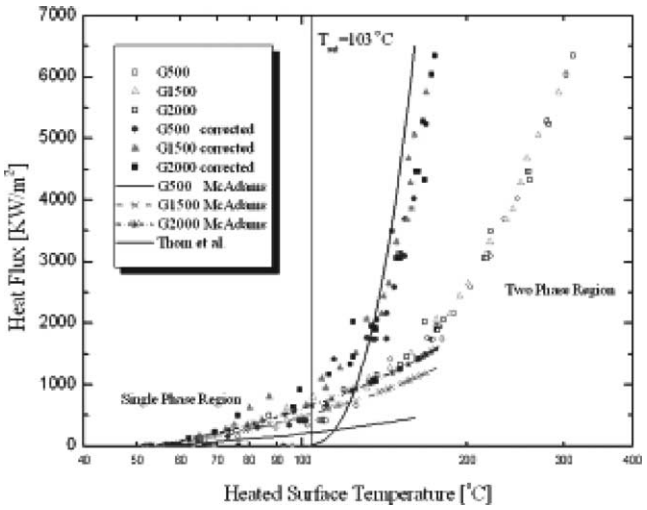

Fig. 5. Boiling curve compared with conventional correlations.

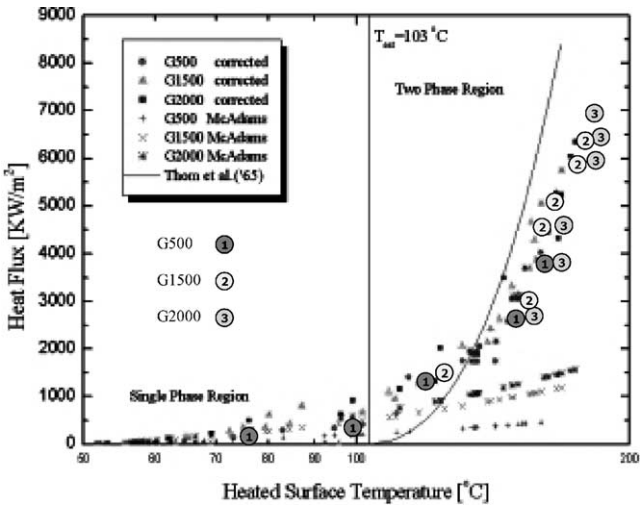

Fig. 6. Conditions of visualization experiment.

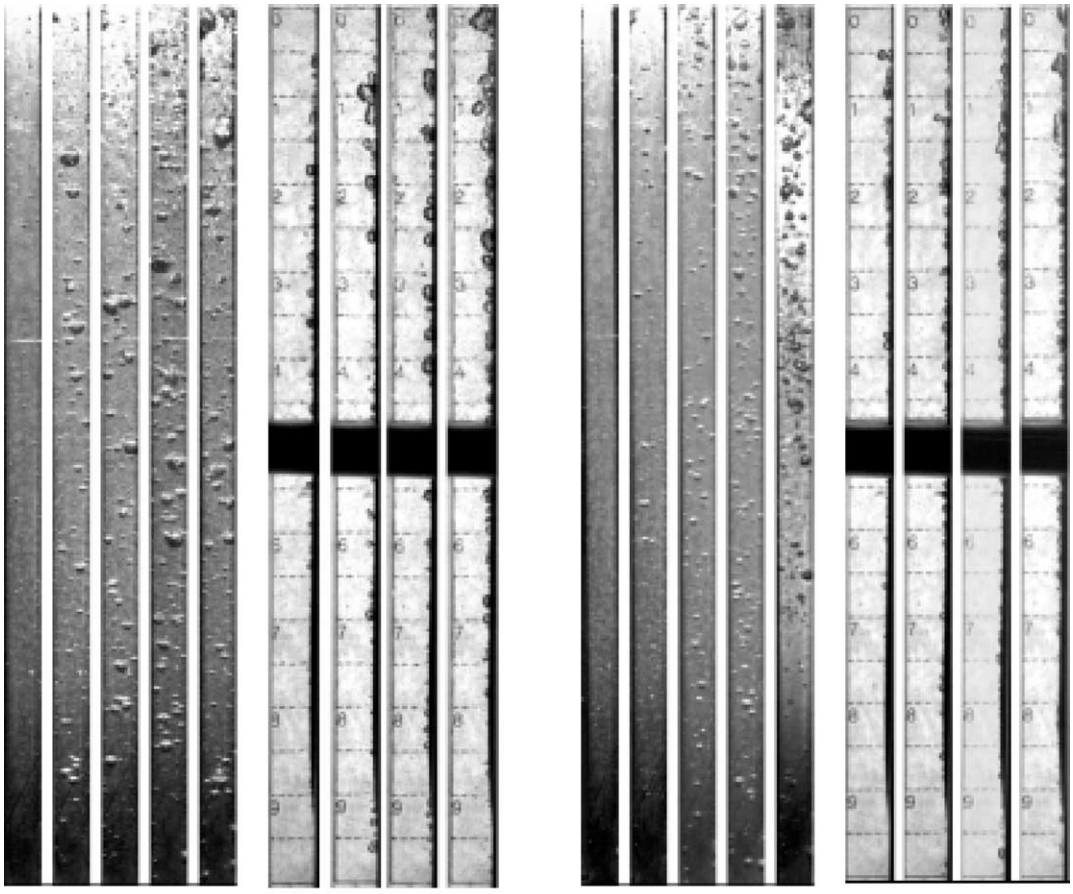

(a) Mass flux 500 kg/m²s

Front observation (width : 4 mm)
0.622, 1.628, 2.45, 2.8, 3.0 MW/m²
Xe = -0.0879, -0.079, -0.0717, -0.0686, -0.0668

Lateral observation (width : 5 mm)
1.616, 2.45, 2.8, 3.3 MW/m²
Xe = -0.0791, -0.0717, -0.0686, -0.0641

(b) Mass flux 2000 kg/m²s

Front observation (width : 4 mm)
2.3 (27.4 %CHF), 3.6 (42.9 %),
4.8 (57.1 %), 5.8 (69%), 6.1 (72.6 %) MW/m²
Xe = -0.0884, -0.0855, -0.0828, -0.0806, -0.0799

Lateral observation (width : 5 mm)
1.216 (14.5 %), 3.6 (42.9 %), 4.8(57.1 %),
5.8(69 %), 6.0 (71.4 %) MW/m²
Xe = -0.0908, -0.0855, -0.0828, -0.0806, -0.0801

Fig. 7. Overall bubble behavior along the heated surface with different heat fluxes.

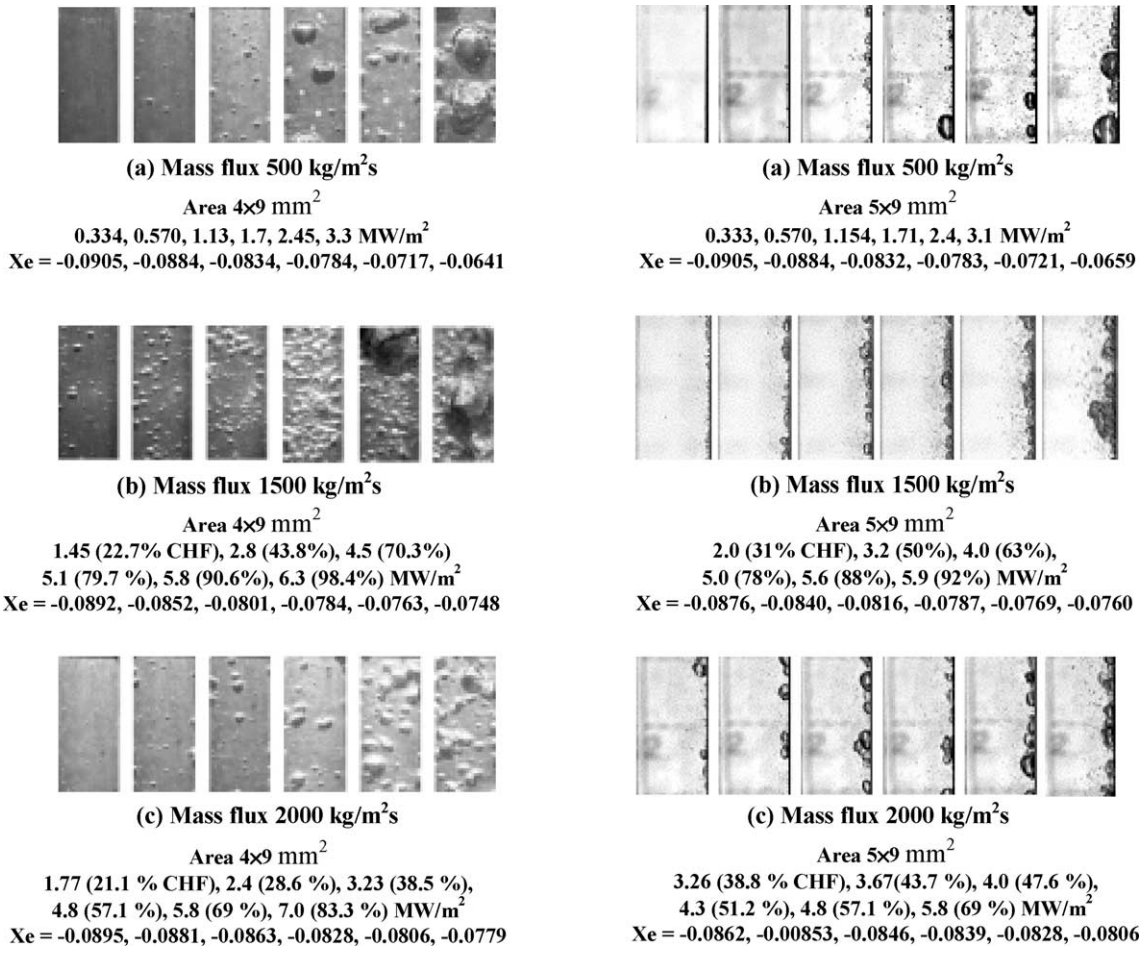

Fig. 8. Effect of mass flux on bubble behavior.

At low heat fluxes, small bubbles with the size of a few microns and the aspect ratio of 1 over 2 grow and collapse at each nucleation site. Those bubbles could move along the heated surface. Sometimes, these bubbles coalesce and form somewhat larger bubbles with sizes of a few bubbles. As heat flux increases over ∼40% CHF, adjacent nucleation sites become more active and bubbles begin to grow in close vicinity. Then adjacent bubbles are coalesced, resulting in big bubbles on the heated surface. The coalescence of bubbles occurs in two ways:

(a) coalescing of 2 ∼ 3 bubbles growing at neighboring nucleation sites, and
(b) merging of bubbles growing at nucleation sites into the larger flowing bubbles.

More nucleation sites and larger vapor clots are observed for the higher heat flux and channel-averaged quality. The size of coalesced bubbles decreases with the increase in mass flux, probably due to the increase in drag force.

Before proceeding to detailed aspects, it is worthwhile to discuss the effect of the exposure time on resulting photographs. Fig. 9 compares photographs taken at the same condition between the exposure times of 1/8700 second and 1/830 second. The photographs for the long exposure indicate the continuous bubbly layer covering the whole heated surface, while discrete and some coalesced bubbles are clearly shown for the shorter exposure time. Application of a sufficiently short exposure time would be crucial to investigate the bubble behavior.

3.3. Bubble behavior near CHF condition

Fig. 10(a) and (b) illustrates the flow structure before and after CHF occurrence for the mass flux of 1500 kg·m^{-2}·s^{-1}. The measurement of CHF is achieved through a sudden rise of the heating plate temperature near exit, and a red-glowed part is observed simultaneously and after power-off, a damaged area is identified. Fig. 10(a) shows the photographs that were continuously taken with the time interval of 0.22 seconds for a high heat flux condition (6.3 MW·m^{-2}, 98.4% CHF). Large vapor clots, with the width of the heated surface and the length of ∼15 mm, are shown near the top of the channel. The time interval between successive pho-

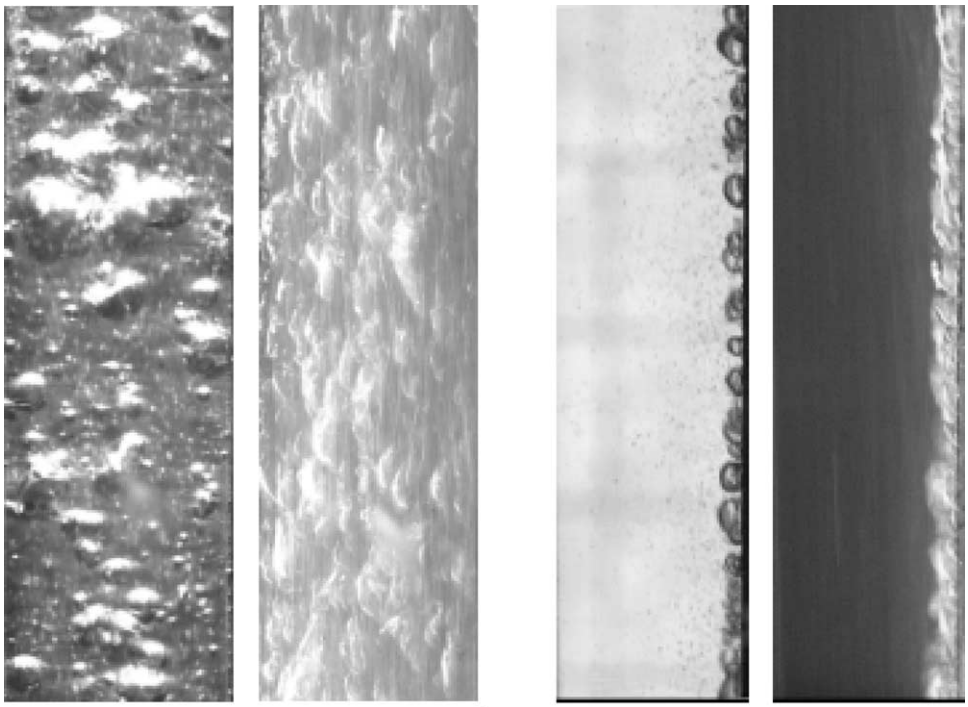

Fig. 9. Photos with different exposure times.

tographs is large enough for a vapor clot to escape, as the vapor clot can move over 100 mm during the time interval. Therefore, the top region in Fig. 10(a) does not represent the growing and escaping behavior of the same vapor clot; instead, it just shows the instantaneous flow structure at arbitrary times. The top region is occupied sometimes by a large wavy vapor clot and sometimes by small or coalesced bubbles. This indicates that large vapor clots would periodically grow and escape from the top region of the heated surface.

Fig. 10(b) shows the flow structure just after the occurrence of CHF at 6.4 $MW \cdot m^{-2}$. The region of DNB occurrence dries out and the dried region expands with time. At the same time, the region occupied by large vapor clots move downward and upward as the heat flux becomes higher near the CHF location due to axial heat conduction from the CHF region with poor heat transfer to cooling water. The heated surface was damaged severely due to the sudden temperature rise.

The CHF occurred during the process of periodic formation of large vapor clots near exit. Considering that a liquid sublayer exists beneath the large vapor clot before CHF, the CHF mechanism at our experimental condition can be related to the dryout of the liquid sublayer under the vapor clot.

3.4. Identification of flow structure

Some photographs of the present work could be considered as the direct evidence of the existence of the superheated liquid layer or liquid sublayer beneath the flowing bubble region. Traditionally, two regions are considered for subcooled flow boiling structure: the bubbly layer near the heated wall and the liquid core region. This has been supported by a variety of experimental works, though detailed information on the bubbly layer has not been obtained. Some investigators proposed the existence of the superheated liquid layer or liquid sublayer between the bubbly layer and the heated surface, which leads to three-layer flow structure: the superheated liquid layer, the flowing bubble layer, and the liquid core. Among them, Larson and Tong [12] developed an analytical model for void fraction distribution in subcooled flow boiling assuming the three layer structure and Lee and Mudawwar [9] developed a mechanistic CHF model assuming a liquid sublayer below a large vapor clot. Recently, Chun et al. [13] also proposed a CHF model based on the concept of the depletion of the superheated liquid layer. However, there has been little experimental work directly showing the existence or characteristics of the liquid layer.

Fig. 12 shows the existence of the liquid sublayer under large coalesced bubbles. The thin layers below coalesced

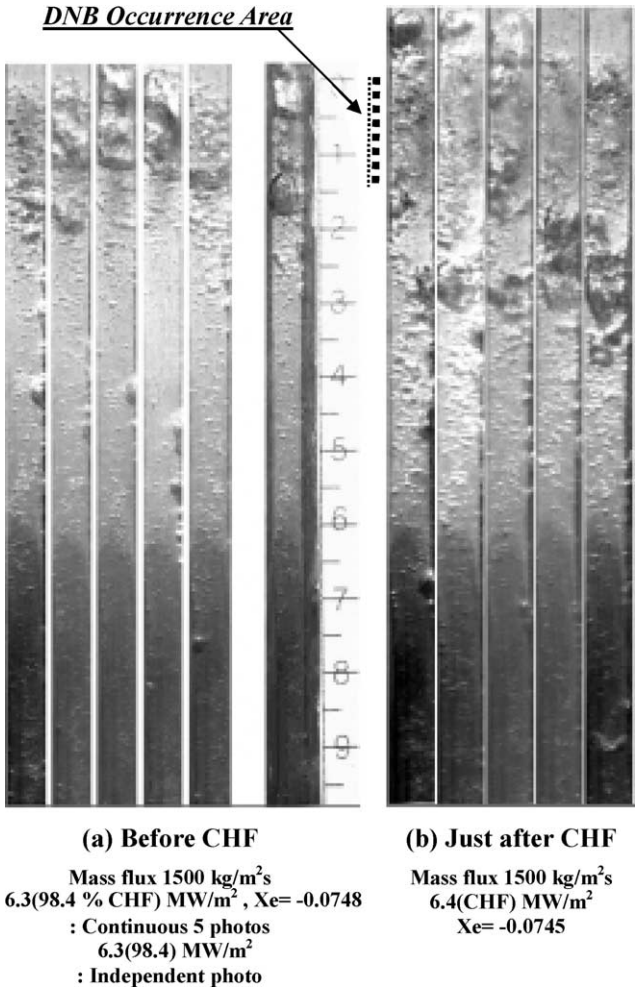

Fig. 10. Flow phenomena near and after CHF.

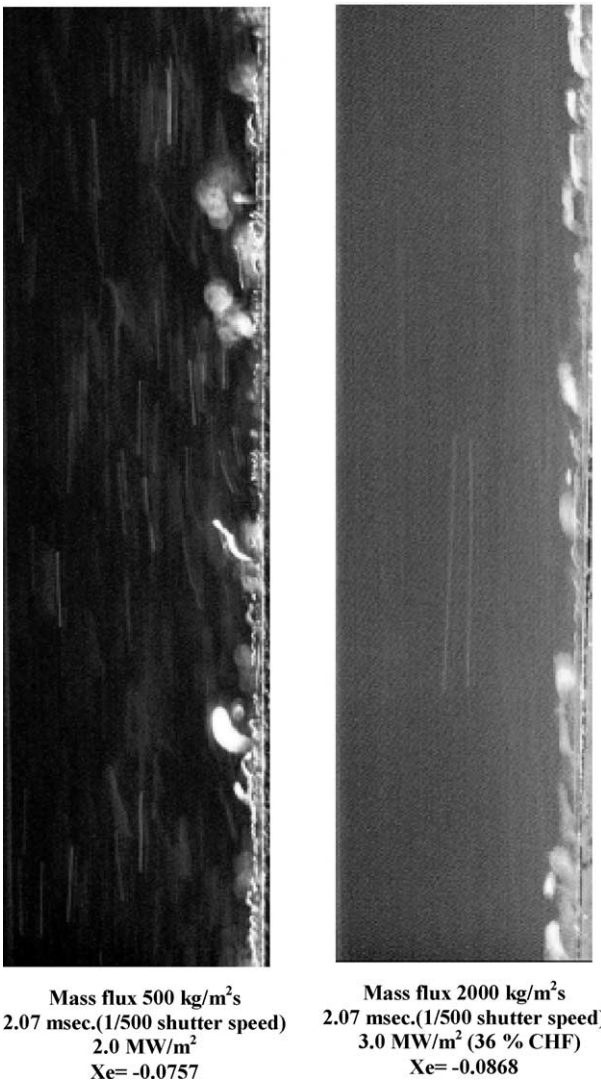

Fig. 11. Photos showing the 3-layer flow structure with a long exposure time.

bubbles in the lateral picture of Fig. 12(a) are considered as the liquid sublayer that is assumed in many CHF modeling, e.g., Lee and Mudawwar [14], Katto [15] and Celata et al. [16]. Fig. 12(b) shows the front visualization with lateral lighting. The bright area behind a bubble would be due to the existence of a liquid sublayer that reflects light less than the coalesced bubble.

More important photographs related to the flow structure were obtained by intentionally applying the long exposure time of 2.07 msec. for mass fluxes of 500 and 2000 $kg{\cdot}m^{-2}{\cdot}s^{-1}$, as shown in Fig. 11. The mass fluxes of 500 and 2000 $kg{\cdot}m^{-2}{\cdot}s^{-1}$ correspond to the single-phase liquid velocity of 0.52 and 2.08 $m{\cdot}s^{-1}$, respectively. The thin, bright lines in the liquid core region correspond to the movement of small bubbles. The coaxial direction and almost the same length of those lines in the liquid core region indicate the coaxial flow of small bubbles at almost the same velocity. The estimated maximum velocities from the line length and exposure time are $\sim$0.69 $m{\cdot}s^{-1}$ for 500 $kg{\cdot}m^{-2}{\cdot}s^{-1}$ and $\sim$2.4 $m{\cdot}s^{-1}$ for 2000 $kg{\cdot}m^{-2}{\cdot}s^{-1}$. The direction of thin lines is different near the heated surface, indicating the movement of bubbles into the liquid core. Larger bubbles slide along the heated surface at much lower velocity than bubbles in the liquid core. Departing of large bubbles from the surface is also seen clearly.

Fig. 11 also shows wavy lines near the heated surface, which are thought to represent small stationary bubbles generating and disappearing at nucleation sites. The wavy lines would be the cumulative images of the caps of attached small bubbles that are generated during the exposure time. It should be noted that only small discrete bubbles are shown for the exposure time of 1/8700 sec, as shown in Fig. 8. In the vicinity of the heated surface, the volume occupied by liquid at an instant would be much larger than that by vapor for moderate heat fluxes. Then the wavy lines would be an indication of the superheated liquid layer with small attached bubbles. Further growth of attached bubbles is prevented by the liquid or vapor flow over the superheated liquid layer. The thickness of the layer is estimated to be $\sim$0.1 mm.

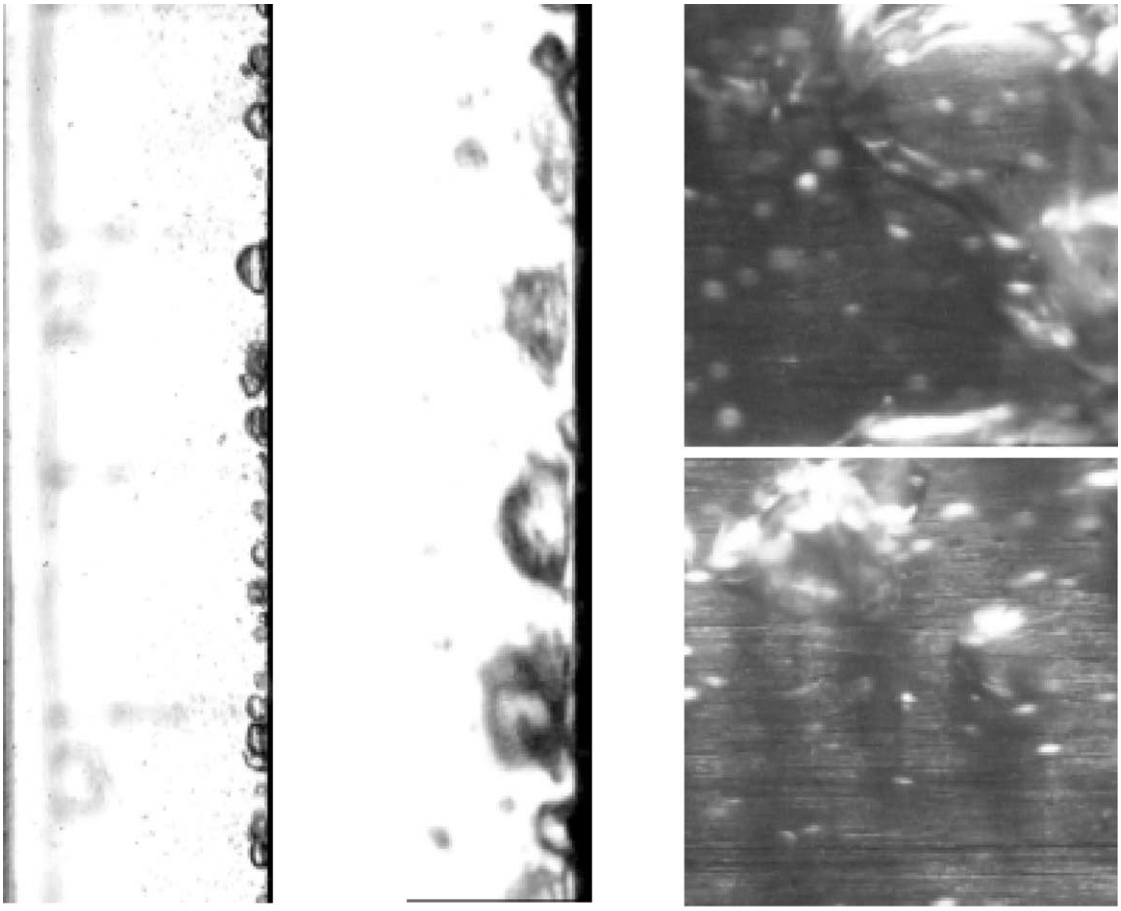

Fig. 12. Liquid sublayer under coalesced bubbles.

We can conclude that our visualization experiment provided a direct experimental evidence for the three-layer structure of subcooled flow boiling under low pressure:

(a) *the superheated liquid layer* with very small bubbles attached on the heated surface,
(b) *the flowing bubble layer* containing vapor clots and small bubbles (coalescence occurs in this layer), and
(c) *the liquid core region* over the flowing bubble layer.

3.5. Further discussion

The visualization experiment in this work has been conducted only for atmospheric pressure condition and the flow velocity region covered is relatively narrow. However, the photographs obtained in this work provide a clear idea of the subcooled flow boiling structure at least for the examined conditions. We also have demonstrated that the digital photographic technique can be useful in visualizing subcooled flow boiling. Further work would be required for different pressure and mass flux conditions possibly with refrigerants. Visualization equipment with improved performance would also enable to measure directly the bubble diameter and the superheated liquid layer thickness.

4. Conclusions

The behavior of near-wall bubbles in subcooled flow boiling has been successfully observed, applying a recent digital imaging technique for subcooled water flow under atmospheric pressure. The main observations are summarized as follows:

(a) Discrete attached bubbles, sliding bubbles, small coalesced bubbles and large coalesced bubbles or vapor clots are observed on the heated surface as the heat flux

is increased from a low value. Significant bubble coalescence is observed for heat fluxes over ∼40% CHF.

(b) At sufficiently high heat flux, three characteristic regions were observed in the heated channel:
  (i) a superheated liquid layer with very small bubbles attached on the heated surface,
  (ii) a flowing bubble layer containing vapor clots and small bubbles, and
  (iii) the liquid core.

(c) The existence of a liquid sublayer under coalesced bubbles has also been identified photographically.

(d) The size of coalesced bubbles decreases with the increase in mass flux. Mass flux has no outstanding effect except for the bubble size and velocity profile. Velocities of bubbles are measured through the exposed line during a long exposure and correspond to single-phase liquid velocities.

(e) The CHF occurs during the process of periodic formation of largely vapor clots near exit, which can be related to the liquid sublayer dryout model.

Further investigation would be required for more reliable identification of DNB mechanisms according to various flow conditions.

Acknowledgements

This work has been supported by Korea Atomic Energy Research Institute (KAERI) through research contract. Special thanks are given to Dr. M.K. Chung, Dr. S.K. Yang, and Mr. S.Y. Chun of KAERI.

References

[1] S.H. Chang, W.P. Baek, Critical Heat Flux—Fundamentals and Applications, Chungmoongak, Seoul, 1997 (in Korean).
[2] S.H. Chang, W.P. Baek, Perspective on critical heat flux research for reactor design and safety, in: Proc. of the 5th Internat. Top. Mtg. on Nuclear Thermal Hydraulics, Operations and Safety (NUTHOS-5), Beijing, China, 1997, AA1.
[3] F.C. Gunther, Photographic study of surface-boiling heat transfer to water with forced convection, Trans. ASME 73 (1951) 115–121.
[4] L.M. Jiji, J.A. Clark, Bubble boundary layer and temperature profiles for forced convection boiling in channel flow, Trans. ASME J. Heat Transfer (1962) 50–58.
[5] L.S. Tong, A.A. Bishop, L.E. Efferding, A photographic study of subcooled boiling flow and DNB of Freon-113 in a vertical channel, ASME Paper (1966), 66-WA/HT-3.
[6] J.E. Galloway, I.A. Mudawwar, CHF mechanism in flow boiling from a short heated wall—I, Examination of near-wall conditions with the aid of photomicrography and high-speed video imaging, Internat. J. Heat Mass Transfer 36 (1993) 2527–2540.
[7] P. Bricard, Souyri, Understanding and modeling DNB in forced convective boiling: A critical review, in: Two-Phase Flow Modelling and Experimentation, 1995, pp. 843–851.
[8] J. Weisman, B.S. Pei, Prediction of critical heat flux in flow boiling at low qualities, Internat. J. Heat Mass Transfer 26 (1983) 1463–1477.
[9] C.H. Lee, I.A. Mudawwar, A. Sesonske, A new critical heat flux model for subcooled two-phase flow through a vertical tube, in: Particular Phenomena and Multiphase Transprot, Miami, Vol. 1, 1986, pp. 425–441.
[10] W.H. McAdams, W.E. Kennel, C.S. Minden, R. Carl, P.M. Picornell, J.E. Dew, Heat transfer at high rates to water with surface boiling, Indust. Engng. Chem. 41 (1949) 1945–1953.
[11] J.R.S. Thom, W.M. Walker, T.A. Fallon, G.F.S. Reising, Boiling in subcooled water during flow up heated tubes or annuli, in: Symposium on Boiling Heat Transfer in Steam Generation Units and Heat Exchangers, Manchester, ImechE (London), 1965, Paper 6.
[12] P.S. Larson, L.S. Tong, Void fraction in subcooled flow boiling, J. Heat Transfer 9 (1969) 471–476.
[13] T.H. Chun, W.P. Baek, S.H. Chang, An integral equation model for critical heat flux at subcooled and low quality flow boiling, Nucl. Engrg. Des. 199 (2000) 13–29.
[14] C.H. Lee, I.A. Mudawwar, A mechanistic CHF model for subcooled flow boiling based on local bulk flow conditions, Internat. J. Multiphase Flow 14 (1988) 711.
[15] Y. Katto, A physical approach to critical heat flux of subcooled flow boiling in round tubes, Internat. J. Heat Mass Transfer 33 (1990) 611–620.
[16] G.P. Celata, M. Cumo, A. Mariani, G. Zummo, A mechanistic model for the prediction of water-subcooled-flow-boiling critical heat flux at high liquid velocity and subcooling, Fusion Technology 29 (1996) 499–511.